SSRG International Journal of Electrical and Electronics Engineering
ISSN: 2348-8379/ https://doi.org/10.14445/23488379/IJEEE-V12I6P109

Volume 12 Issue 6, 118-124, June 2025

Original Article

Design and Performance Analysis of Slotted-Rotor-Tooth Switched-Reluctance-Motor for EV Applications using FEA Tool

Mahesh A. Patel[1], Swapnil N. Jani[2]

[1,2]*Department of Electrical Engineering, Institute of Technology, Nirma University, Ahmedabad, Gujarat, India.*

[1]*Corresponding Author : er.maheshpatel@gmail.com*

Received: 06 April 2025 Revised: 08 May 2025 Accepted: 07 June 2025 Published: 30 June 2025

Abstract *- Switched-Reluctance Motors (SRMs) have garnered significant interest in the realm of electric vehicle (EV) propulsion due to their unique characteristics, including ease of use, high torque density, and speed regulation capabilities. However, challenges persist, particularly in optimizing efficiency and addressing torque ripple problems associated with traditional topologies. This paper introduces a new slotted rotor-tooth switched reluctance motor (SRT-SRM) design, offering reduced weight, enhanced cooling capability, and cost savings over traditional switched reluctance motors (SRMs). The preliminary dimensions of the conventional SRM have been calculated and analyzed through a time-stepping (transient) 3-D Finite Element Analysis (FEA). In a novel topology of SRT-SRM, rotor barriers have been inserted into each rotor pole to get the benefits of higher performance of the SRM motor. It emphasizes the iterative optimization process, wherein topology modifications are implemented to minimize torque ripple and improve overall performance. The results of a novel topology (SST-SRM) have been compared with conventional SRM for validation.*

Keywords *- Electric Vehicles (EVs), Finite Element Analysis (FEA), Switched-Reluctance-Motor (SRM), Slotted-Rotor-Tooth (SRT).*

1. Introduction

One of the key reasons for the development of electric vehicles is the effect of climate change. Since electric vehicles have no exhaust emissions, they drastically lower the transportation sector's carbon impact. EVs often produce lower overall emissions than conventional internal combustion engine vehicles, even when taking the power generation source into account [1]. Since electricity is usually less expensive than gasoline or diesel, EV owners could get the financial benefits of fuel and have fewer moving components. EVs also require less maintenance, which lowers long-term maintenance costs [2].

Having electric cars is essential to a sustainable future. Extensive research into reliable and efficient electric motor technology has been encouraged by the rising demand for electric vehicles (EVs). Permanent magnet synchronous motors (PMSMs) and permanent magnet brushless DC motors (PMBLDCs) have been widely used [3] in recent times, but the specific limitations of these machines have led researchers to opt for the newer topology. Various advanced electric motors have been compared for EV and EHV applications in [4]. Permanent magnets employed in PM motors are costly and vulnerable to supply chain fluctuations. The mining and processing of these commodities can give rise to environmental concerns. PMSMs are the most widely used motor in various applications, i.e., 3-wheelers and 4-wheelers, because of their benefits of higher power density and higher efficiency. Similarly, PMBLDCs have limitations related to high-speed performance and thermal management issues.

The switched reluctance motor does not use permanent magnets, and as a strong contender among all-electric motor technologies, it has been receiving more and more attention for EV applications [5]. Its construction is simple, with no permanent magnets and no rotor winding. It offers various benefits, such as lower cost and higher efficiency at a great speed under challenging conditions. It has a great withstand capacity against phase failure due to its fault-tolerant architecture. The problems associated with SRMs, including higher noise and torque ripple, are being addressed through developments in power electronics and control technologies [6]. SRMs have become viable because of their wide speed range, fault tolerance, and robust, straightforward design [7]. There are numerous approaches to increasing torque in SRM. The slotted stator tooth SRM has been investigated for higher torque. It has been investigated how various stator and rotor pole arcs affect torque characteristics. Average torque may be improved, and torque ripple can be decreased with the right pole arc combinations. Various notching and shaping techniques on stator and rotor poles have been investigated to maximise flux waveforms and minimise torque ripple.

Various topologies are addressed in the literature to minimize the torque ripple of SRM by different rotor and stator pole combinations. The torque characteristics have been studied using the finite element analysis in [8]. The systematic design procedure has been studied in [9]. The cost-effective and lightest-weight SRM has been explored in [10, 11] with electromagnetic analysis. Several slot shapes - such as rectangular, trapezoidal, and curved - have been studied to maximise flux and minimise leakages.

In this paper, the rotor pole shape of a conventional topology of SRM has been modified by introducing barriers to diminish the torque ripple and better the torque profile of the proposed SRT-SRM. In the presented research, the rotor barriers are inserted in each rotor pole to enhance the benefits of rotor barriers. The rotor barriers are introduced in the synchronous reluctance motor to accommodate the PMs in the barrier (PMA-SynRM) motor to reduce torque ripples.

The number of barriers inserted into the rotor teeth directly affects the motor's average torque and torque ripple. In the proposed design, one barrier is introduced for benefits, i.e., cost-effectiveness, for better cooling and weight reduction. The magnetic flux distribution torque properties in SRT-SRMs have been analyzed using transient (time stepping) 3-D finite element analysis. This leads to improved torque density and a smoother torque ripple, making SST-SRMs a viable option for EV applications. The performance of these motors can be further improved, and the adoption of EVs will be accelerated by ongoing research for design optimization and validation through a prototype design.

The basic construction and workings of SRM are discussed in Section II. A novel topology of SRT-SRM has been developed with initial analytical design parameters in Section III and analyzed through the transient (time-stepping) 3-D finite element analysis [12, 13] for validation in Section IV. It emphasizes the iterative optimization process, wherein topology modifications are implemented to reduce torque ripple and improve overall performance. Concluding remarks and future scope have been discussed in Section V.

2. Construction of a Switched-Reluctance Motor

An SRM generates torque by virtue of its movable component's behaviour to shift to a position where the excited windings' inductance is at maximum. The stator often has a larger number of poles than the rotor. Rotor and stator poles, rotor and stator back-iron, and coils are mounted on the stator poles as depicted in Figure 1. The motor's single phase is created by connecting the stator windings, which are positioned on opposing poles, in series or parallel.

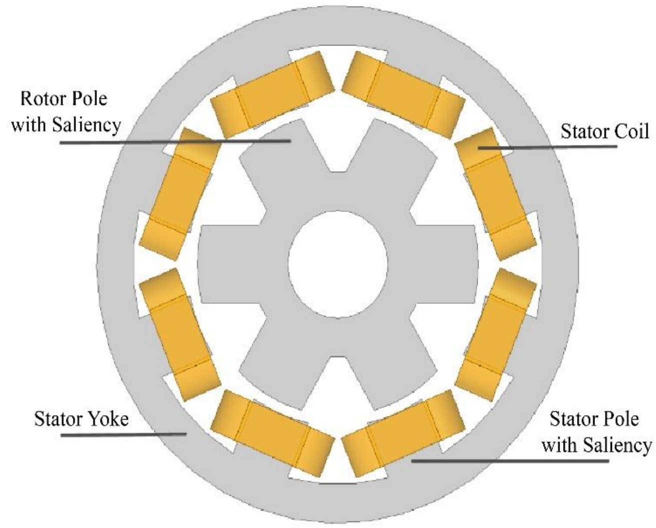

Fig. 1 Construction of switched-reluctance motor

Commonly used stator and rotor pole combinations are 6/4, 8/4, 10/6, and 12/6. Designs with more stator/rotor poles could minimize the torque ripple. The rotating element naturally moves to the position of least reluctance upon excitation in the magnetic circuit. Two rotor poles align with two stator poles, while the other rotor pole pair is misaligned with another stator pole set. The stator poles are re-energized to realign the rotor poles [14]. While deriving the fundamental equivalent circuit for an SRM, mutual inductance between phases is typically neglected. The per-phase applied voltage equals the sum of the flux linkage rate and resistive drop. This voltage expression is shown below.

$$V = R_s . i + L(\theta, i) . \frac{d_i}{d_t} + i . \omega_m . \frac{dL(\theta,i)}{d\theta} \quad (1)$$

The terms on the right of the equations stand for the resistive, inductive, and induced EMF voltage drops and follow the same equation of the series-excited DC motor voltage equation. The equation finds the power developed by the machine,

$$P_{out} = m . K_{eff} . K_{dt} . V . i \quad (2)$$

Where K_{eff} is the motor efficiency, and K_{dt} is the duty cycle, which is given by,

$$K_{dt} = m . \theta . P_r / 360 \quad (3)$$

Where, θ is an angle for increasing the inductance waveform. The final output power equation can be written as,

$$P_{out} = K_{eff} . K_{dt} \left(\frac{\pi^2}{120}\right) . \left(1 - \frac{1}{\sigma_s . \sigma_u}\right) . B . A_s . D^2 . L . n \quad (4)$$

Where n is the shaft speed in rpm of the rotor. The torque could be found with the equation,

$$T_{out} = K_{eff}.K_{dt}.(k_1).(k_2).B.A_s.D^2.L \tag{5}$$

3. Analytical Design of Switched-Reluctance Motor

SRM should include a base speed specification since it typically functions as a variable speed machine. At base speed, the motor must provide the rated torque and, thus, the rated output power. As shown in Figure 2, initial design parameters need to be determined through analytical calculations [15].

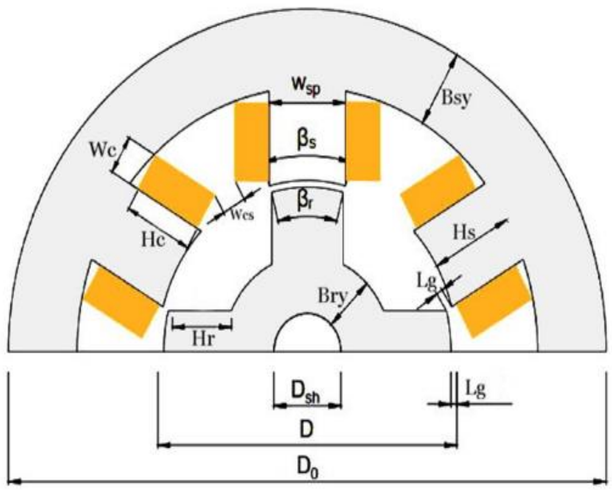

Fig. 2 Dimensions of switched-reluctance motor

Substituting $L = k.D$, power equation becomes,

$$P_{out} = k_2.D^3 \tag{6}$$

Reasonable values can be used to begin the iterative design process. The range of k_2 is given by the operating point is,

$$0.65 < k_2 < 0.75 \tag{7}$$

It is possible to consider the aligned position's flux density *(B)* to represent the upper limit permitted for core material. In amp-conductors, the specific electric loading range between,

$$20000 < A_s < 95000 \tag{8}$$

It is reasonable to assume the duty cycle k_{dt} is one at the beginning. The bore diameter *D* is determined using the above factors. Air gaps in machines with lower power ratings range from 0.18 to 0.25 mm. Air gaps on higher-rated equipment could range from 0.3 to 0.5 mm. The length-to-bore *k* ratio need not be chosen randomly; it depends on the customer's requirements and space availability. The following formulas can be used to determine the number of turns for a given electric loading (A_s),

$$A_s = m.i.\frac{2T_{ph}}{\pi.D} \tag{9}$$

The size of the conductor is selected to fill the existing area available for winding. Based on the motor's cooling method, the current density is calculated. If the outer diameter is not fixed, the winding area is determined using the number of turns, conductor cross-section, and insulation thickness. The stator back-iron thickness (B_{sy}) depends on its peak flux density. The back-iron carries roughly half the flux density of the stator poles. Pole flux density must be considered when selecting stator pole arcs. The stator pole width (W_{sp}) is given below.

$$W_{sp} = D.\sin\left(\frac{\beta_s}{2}\right) \tag{10}$$

Consequently, $0.5W_{sp}$ must be the minimum thickness of the back-iron Bsy. Because mechanical robustness and vibration reduction are considered, its value may fall between,

$$W_{sp} > B_{sy} > 0.5.W_{sp} \tag{11}$$

The conductor's cross-sectional area defines the stator coil's width (W_c) and length (H_c). This area is calculated based on (T_{ph}) and the current density. Let (Wcs) represent the width or spacing required between two adjacent coils at the bore slot. The stator coil area is expressed using the area of conductors and the number of turns, as shown in the equation below.

$$H_c.W_c = ac.\frac{T_{ph}}{2} \tag{12}$$

The coil width (W_c) can be obtained from,

$$W_c = \frac{\pi.D - P_s\left[\beta_S.\frac{D}{2}\right] + W_{cs}}{2P_s} \tag{13}$$

The coil height (H_c) can be calculated,

$$H_c = ac.\frac{T_{ph}}{2.W_c} \tag{14}$$

The height of the stator pole (H_s) is approximately equal to the height of the coil, although securing the coil requires a small space at the pole face. After considering these factors and the need for a shorter pole length, the pole height is defined by $H_c < H_s < 1.4H_c$.

$$H_s = (D_o - 2B_{sy} - D)/2 \tag{15}$$

If the outside diameter in electric vehicles is limited to a specific value, the design is derived from the outer to the inside dimensions. NEMA and other organizations may not assign frame numbers to machines used in variable speed applications. The outer diameter of the stator lamination can then be calculated by adding the thickness of the back iron and pole heights to the design details. It is provided by,

$$D_o = D + 2B_{sy} + 2H_s \qquad (16)$$

Operating flux density and structural strength define the rotor back-iron thickness (Bry). It does not need to match the stator back-iron thickness, be half the stator pole width, or satisfy a minimum value. The wider interpolar air gap must be considered while selecting a range of values. Shorter rotor poles are also better since they reduce rotor vibration. The rotor back-iron thickness (W_{rp}) ranges from $0.5W_{sp} < W_{ry} < 0.75W_{sp}$.

The rotor pole height (H_r) can be expressed as follows if the rotor shaft diameter (D_{sh}), rotor back-iron thickness (B_{ry}), air gap length (L_g), and bore diameter (D) are known,

$$H_r = \frac{D - 2L_g - D_{sh} - 2B_{ry}}{2} \qquad (17)$$

All necessary dimensions have been calculated and tabulated in Table 1.

Table 1. Specifications and main dimensions of the SRM motor

Parameters	Value
Stator Pole	8
Rotor Pole	6
Stator Lamination Diameter	198 mm
No. of Phases	4
Stator Bore Diameter	130 mm
Height of Stator Pole	25 mm
Stator Pole Arc (in degree)	23°
Height of Rotor Pole	15 mm
Rotor Pole Arc (in degree)	21°
Air-gap Length	0.25 mm
Axial Length	180 mm
Shaft Diameter	50 mm
Turns per Phase	25
Rotor Speed	3000 rpm
DC Bus Voltage	400 V
Peak Current	100 A

4. Analysis of Conventional Switched-Reluctance Motor

4.1. Finite Element Analysis of a Conventional SRM

A time-stepping three-dimensional (3D) finite element analysis has been carried out for a conventional switched reluctance motor (SRM). Figure 3 shows the traditional SRM's flux density vector plot. All fluxes would pass through the air gap area when the stator and rotor poles are perfectly aligned, which results in very low reluctance. Similarly, during unaligned conditions, the reluctance is very high, and the fluxes that travel through the air gap are less and more leakage fluxes can be observed at the corners of the stator and the rotor poles.

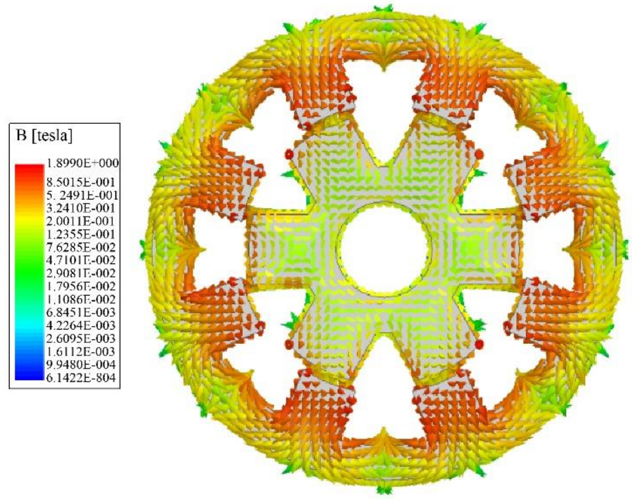

Fig. 3 Flux density vector plot of conventional SRM

The linear winding pattern for a traditional SRM and the coil configuration surrounding an SRM's stator poles are depicted in Figure 4.

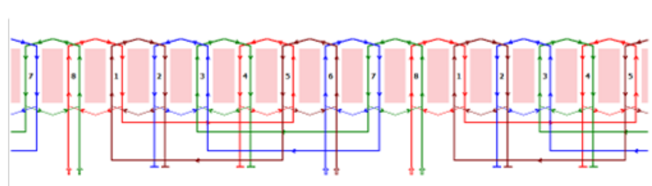

Fig. 4 Linear pattern of winding of conventional SRM

The stator poles are probably represented by the digits 1–8. The colored arrows show the current flow in the windings. This is essential for figuring out the direction of the magnetic field. The stator poles where the magnetic flux will concentrate are probably represented by the red-shaded sections. The windings' routes, joined by the coils around the poles, are shown by wave-shaped lines. Understanding the connection between rotor position, current, and the resulting torque is necessary to analyse FEA (Finite Element Analysis) data for a torque plot in Figure 5 in an SRM. It displays the variation in torque generated by the SRM as the rotor turns. Because of the rotor's propensity to shift to a location of minimum reluctance, SRMs generate torque.

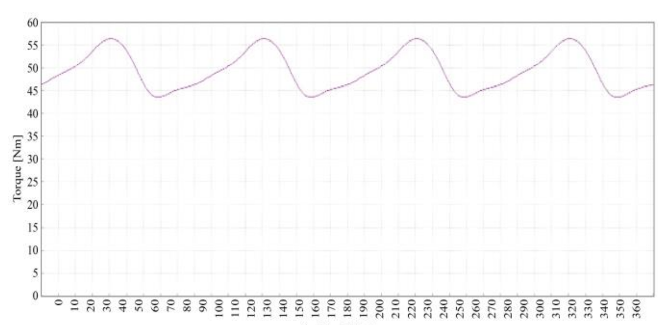

Fig. 5 Torque plot of conventional SRM

The torque curve's shape is critical in assessing the motor's performance, including torque ripple. Torque ripple can be measured with the help of FEA results, which is crucial for determining how smooth the motor is and whether it is appropriate for applications that call for exact motion control.

4.2. Analysis of a Modified Novel Topology of SRT-STM

The conventional geometry has been modified by inserting the rotor barrier in the rotor to enhance the torque of the novel topology. Figure 6 shows the 3-D modified novel topology.

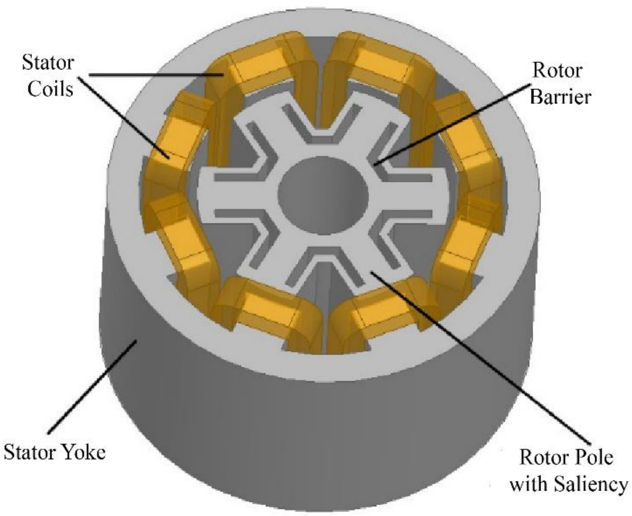

Fig. 6 Construction of a novel topology of SRT-SRM

A novel SRT-SRM's performance characteristics require analyzing the flux linkage plot as illustrated in Figure 7, which FEA has produced. The idea that the slotted rotor design increases the effective air-gap area and changes the flux path, resulting in a higher flux linkage and a lower reluctance, has been analyzed through finite element analysis (FEA) simulations.

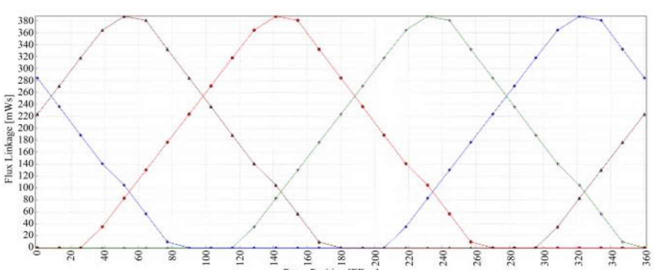

Fig. 7 Flux linkages plot of SRT-SRM

For each phase, the flux linkage is typically plotted against the rotor position, with the rotor position on the x-axis and the flux linkage on the y-axis. The resulting flux linkage curve for SRM is generally nonlinear. This nonlinearity arises because the reluctance changes as the rotor moves in and out of alignment with the stator poles. When the rotor and stator poles are aligned, the reluctance is at its lowest, and the flux linkage is at its maximum. The phase winding's inductance is indicated by the flux linkage curve's slope. Figure 8 shows the flux linkage in an SRT-SRM as it varies with rotor position and current levels.

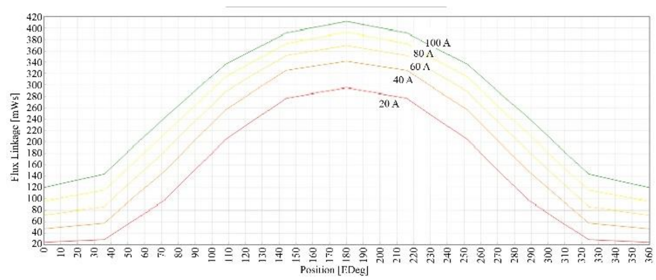

Fig. 8 Flux linkages with rotor position at different current loading of SRT-SRM

For SRM design and control, this analysis is crucial. The flux linkage for a particular phase at a different current level (e.g., 20A, 40A, 60A, 80A, 100A) is represented by each curve. The usually nonlinear curves show reluctance changes when the rotor aligns and misaligns with the stator poles. The flux linkage grows as the current in a phase winding increases for a specific position of the rotor. This is mainly because a higher current creates a stronger magnetic field. Saturation effects may be observed at very high currents. The curves flatten down at this point because the magnetic material can no longer" hold" any more flux. By examining the slope of a flux linkage curve at a specific rotor position, one can ascertain the inductance of the winding at that position. The speed at which the flux linkage varies with the rotor position is directly proportional to the torque generated by an SRM. A thorough grasp of the electromagnetic behavior of the SRM has been analyzed by closely examining the flux linkage vs. rotor position plot for various current levels. This information is crucial for maximizing the motor's control and design to satisfy certain application needs. The comparison of flux density plots of a conventional SRM and an SRT-SRM is shown in Figure 9.

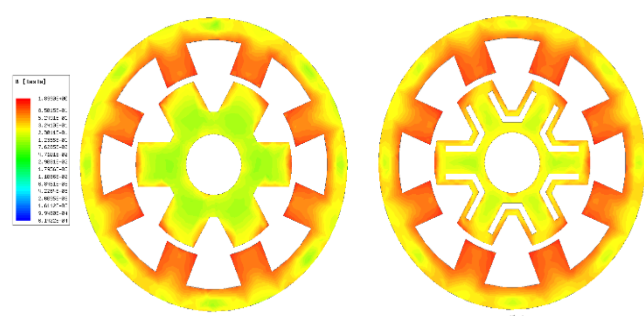

Fig. 9 Comparison of the flux density plot of (a) Conventional SRM, and (b) A novel SRT-SRM.

The comparison of torque plots for conventional SRM and SRT-SRM is depicted in Figure 10. The torque varies as the rotor poles shift in and out of line with the stator poles.

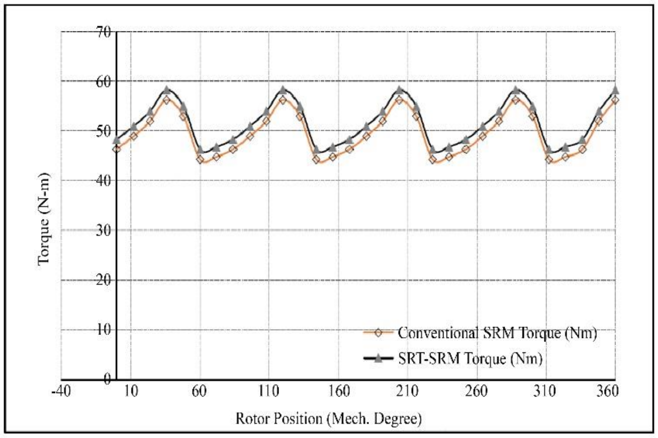

Fig. 10 Comparison of the torque plot of a conventional and a novel SRT-SRM

One significant observation is that the SRT-SRM shows a noticeable reduction in torque ripple compared to the conventional SRM. The average torque in the proposed SRT-SRM is higher than in the conventional SRM by keeping the same design dimensions.

The torque ripples have been reduced by 10 percent of the average torque obtained in the proposed novel topology of SRT-SRM. More accurate measurements or statistics are required to substantiate the possibility that the SRT-SRM has a slightly higher average torque in specific areas. The decrease in torque ripple observed in the proposed SRT-SRM demonstrates that the machine's performance meets the requirements for electric vehicle applications.

5. Conclusion

Various types of SRMs have been reviewed through existing literature and found suitable for electric vehicles due to their features. The dimensions have been calculated using numerical equations and used to analyze 3-D FE analysis. The concept presented with a barrier inserted into rotor poles has been analyzed for the torque characteristics. The slotted rotor tooth arrangement significantly improves torque by efficiently increasing flux linkage and lowering torque ripple. These results highlight the potential of SRT-SRMs as a means of improving efficiency and performance in subsequent electric cars. Through this design, torque density is raised, and torque ripple is decreased, improving vehicle acceleration performance. Thermal analysis can be carried out for future research prospects of the proposed SRT-SRM topology to predict thermal losses due to the generation of heat. It could help to improve the accuracy of the prediction of generator performance. To further enhance the effectiveness and efficiency of the SRT-SRM, more slot geometry optimization and investigation of sophisticated control strategies are advised.

Acknowledgments

I want to thank Nirma University, Ahmedabad, for providing the platform for computational soft tools to enhance the research.

References

[1] Hajo Ribberink, and Evgueniy Entchev, "Electric Vehicles - A 'One-Size-Fits-All' Solution for Emission Reduction from Transportation," *2013 World Electric Vehicle Symposium and Exhibition (EVS27)*, Barcelona, Spain, pp. 1-7, 2013. [CrossRef] [Google Scholar] [Publisher Link]

[2] Pankaj Kumar Dubey et al., "A State of the Art of Recent Trends in Electric Vehicles Planning," *Smart Electric and Hybrid Vehicles: Advancements in Materials, Design, Technologies, and Modeling*, pp. 159-176, 2024. [CrossRef] [Google Scholar] [Publisher Link]

[3] Tushar Suryavanshi et al., "Comparative Analysis of Switched Reluctance Motor Drive with Different Sources for Electric Vehicle," *2024 IEEE 3rd International Conference on Electrical Power and Energy Systems (ICEPES)*, Bhopal, India, pp. 1-6, 2024. [CrossRef] [Google Scholar] [Publisher Link]

[4] Zhi Yang et al., "Comparative Study of Interior Permanent Magnet, Induction, and Switched Reluctance Motor Drives for EV and HEV Applications," *IEEE Transactions on Transportation Electrification*, vol. 1, no. 3, pp. 245-254, 2015. [CrossRef] [Google Scholar] [Publisher Link]

[5] N. Zabihi, and R. Gouws, "A Review on Switched Reluctance Machines for Electric Vehicles," *2016 IEEE 25th International Symposium on Industrial Electronics (ISIE)*, Santa Clara, CA, USA, pp. 799-804, 2016. [CrossRef] [Google Scholar] [Publisher Link]

[6] B. Hemanth Kumar et al., "Control of Modified Switched Reluctance Motor for EV Applications," *2022 Trends in Electrical, Electronics, Computer Engineering Conference (TEECCON)*, Bengaluru, India, pp. 123-127, 2022. [CrossRef] [Google Scholar] [Publisher Link]

[7] L. Ananda Padmanaban, and P. Saravanan, "Design, Analysis and Comparison of Switched Reluctance Motors for Electric Vehicle Application," *Automatika: Journal for Control, Measurement, Electronics, Computing and Communications*, vol. 64, no. 2, pp. 239-247, 2023. [CrossRef] [Google Scholar] [Publisher Link]

[8] Kazuhiro Ohyama et al., "Design using Finite Element Analysis of Switched Reluctance Motor for Electric Vehicle," *2006 2nd International Conference on Information and Communication Technologies*, Damascus, Syria, vol. 1, pp. 727-732, 2006. [CrossRef] [Google Scholar] [Publisher Link]

[9] Pavol Rafajdus et al., "Design Procedure of Switched Reluctance Motor used for Electric Car Drive," *2014 International Symposium on Power Electronics, Electrical Drives, Automation and Motion*, Ischia, Italy, pp. 112-117, 2014. [CrossRef] [Google Scholar] [Publisher Link]

[10] Li Weili, Sheng Man, and Huo Fei, "Optimal Design and Finite Element Analysis of Switched Reluctance Motor for Electric Vehicles," *2008 IEEE Vehicle Power and Propulsion Conference*, Harbin, China, pp. 1-5, 2008. [CrossRef] [Google Scholar] [Publisher Link]

[11] Alireza Siadatan, Narges Fatahi, and Mahsa Sedaghat, "Optimum Designed Multilayer Switched Reluctance Motors for use in Electric Vehicles to Increase Efficiency," *2018 International Symposium on Power Electronics, Electrical Drives, Automation and Motion (SPEEDAM)*, Amalfi, Italy, pp. 304-308, 2018. [CrossRef] [Google Scholar] [Publisher Link]

[12] A.L. Oliveira, A. Pelizari and A.J. Sguarezi Filho, "Finite Element Analysis Simulation of Switched Reluctance Motor Drive," *IEEE Latin America Transactions*, vol. 16, no. 7, pp. 1928-1933, 2018. [CrossRef] [Google Scholar] [Publisher Link]

[13] Hussein Ali Bardan, and Amer Mejbel Ali, "Analysis of Switched Reluctance Motor based on RMXprt, Maxwell2D and Matlab," *2022 2nd International Conference on Advances in Engineering Science and Technology (AEST)*, Babil, Iraq, pp. 675-680, 2022. [CrossRef] [Google Scholar] [Publisher Link]

[14] Lavanya Vadamodala et al., "A Modified Geometry Based Analytical Model of Switched Reluctance Motor for Rapid Design Process," *IEEE Transactions on Industry Applications*, vol. 61, no. 3, pp. 3753-3763, 2025. [CrossRef] [Google Scholar] [Publisher Link]

[15] Sufei Li et al., "Modeling, Design Optimization, and Applications of Switched Reluctance Machines-A Review," *IEEE Transactions on Industry Applications*, vol. 55, no. 3, pp. 2660-2681, 2019. [CrossRef] [Google Scholar] [Publisher Link]